Adsorption-reduction of Cr(VI) onto unmodified and phytic acid-modified carob waste: Kinetic and isotherm modeling

Kenza Bouaouina, Alexandre Barras, Nacer Bezzi, Mohammed Amin, Sabine Szunerits, Rabah Boukherroub

Adsorption-reduction of Cr(VI) onto unmodified and phytic acid-modified Carob waste: Kinetic and isotherm modeling

Kenza Bouaouina,[a,b] Alexandre Barras,[b] Nacer Bezzi,[a] Mohammed A. Amin,[c] Sabine Szunerits[b] and Rabah Boukherroub[b*]

[a] *Laboratoire de Technologie des Matériaux et de Génie des Procédés (LTMGP), Université de Bejaia, 06000 Bejaia, Algérie*

[b] *Univ. Lille, CNRS, Centrale Lille, Univ. Polytechnique Hauts-de-France, UMR 8520 - IEMN, F-59000 Lille, France*

[c] *Department of Chemistry, College of Science, Taif University, P.O. Box 11099, Taif 21944, Saudi Arabia*

*To whom correspondence should be addressed: Rabah Boukherroub (rabah.boukherroub@univ-lille.fr; Tel. +333 62 53 17 24)

Abstract

Carob waste (CW) is an agro-biomass material abundant in nature with potential use for eco-friendly remediation. However, like many biomass-based adsorbents, it suffers from its low adsorption capacity for organic/inorganic pollutants. Therefore, modification using physical and/or chemical means is commonly applied to improve the adsorptive properties of biomass-based adsorbents. In this study, carob waste (CW) and carob waste functionalized with phytic acid (PA-CW), as an ecofriendly product, were applied for the first time for Cr(VI) elimination. Various methods were applied for the material characterization like Fourier-transform infrared spectroscopy, powder X-ray diffraction (PXRD), thermogravimetric analysis (TGA and DTG), X-ray photoelectron spectroscopy (XPS), specific surface area and porosity measurements. The results proved that both CW and PA-CW own appropriate features for efficient adsorption. Bach experiments revealed that the optimum parameters for Cr(VI) (100 mg/mL) removal at 25°C were pH 2, 0.05 g and 0.025 g as adsorbent dose for CW and PA-CW, respectively, over 120 min contact time. The kinetic of adsorption was well-described by the pseudo-second order model, whereas the isotherm modeling fitted well the modified Langmuir model. CW and PA-CW achieved respectively maximum adsorption capacities of 212.4 and 387.9 mg/g, which are among the highest values so far reported for biomass-based adsorbent materials. These results confirmed that CW and PA-CW could be alternative cost-effective adsorbents even for high concentrations of Cr(VI) in industrial wastewaters along with their reduction capacity.

Keywords: Carob waste; Phytic acid; Cr(VI) adsorption; Kinetic-isotherm; Thermodynamic modeling.

1. Introduction

No one doubts that industrial development led to the well-being of human life. However, this development created a large water pollution by different industrial contaminants, causing damage to nature and living organisms. Among these pollutants, heavy metals are considered recently as an urgent concern (Jaishankar et al., 2014; Mishra and Bharagava, 2016). In addition to human activities such as textile, mining extraction industries and nuclear power, heavy metals could be from natural origin like soil erosion and volcanic activities (Akpor et al., 2014). Among these heavy metals, chromium (Cr) accounts for the seventh most abundant element on earth (Jaishankar et al., 2014). It is commonly used in paint, textile dyes, chemicals, metal corrosion inhibition, and pharmaceuticals. Chromium is present in the environment in two stable oxidation forms, Cr(VI) and Cr(III). Owing to its high stability, solubility and mobility, Cr(VI) is more toxic compared to Cr(III). As a consequence, Cr(VI) can impact negatively enzyme activity and plant growth (Akpor et al., 2014). It is considered as one of the 17 elements that cause a health threat to human (Mishra and Bharagava, 2016). Therefore, Cr(VI) removal represents a primordial issue for researchers in the recent decade. Several approaches have been applied for Cr(VI) elimination such as ion exchange (Ye et al., 2016), membrane separation (Li et al., 2018), electrocoagulation (Vasudevan and Lakshmi, 2011; GracePavithra et al., 2019), adsorption (Halouane et al., 2017), photocatalysis (Dehghani et al., 2016), and solvent extraction (Ning et al., 2014).

Adsorption efficiency has been approved and chosen in several studies, owing to its low cost and simple design. Currently, non-conventional adsorbents like agricultural wastes compete with the usual ones (charcoal, zeolites, and clays) in heavy metals removal, because they are abundant and not expensive. Among these, groundnut shell (Babarinde and Onyiaocha, 2016), acorn waste (Kuppusamy et al., 2017), pine cone (Almendros et al., 2015),

fruit peels and sugarcane bagasse (Chao et al., 2014), sawdust (Ouafi et al., 2017), and many other biomass-based materials have been successfully applied for Cr(VI) elimination from wastewater.

Even though agro-waste materials represent an appealing alternative to synthetic ones for Cr(VI) adsorption, their adsorption capacity in raw form is generally feeble to compete with the existing ones. Therefore, natural adsorbents are not used in their raw nature, but different treatments are applied on the adsorbents' surface to enhance their adsorption capacity by increasing their porosity, specific space area or by the introduction of new actives sites. These treatments are commonly based on chemical or physical agents and processes such as acids, bases, high temperature, etc. (Schwantes et al., 2016; Heidarinejad et al., 2020). According to our best knowledge, only a few studies were devoted on the nature and toxicity of the agents used toward the environment. To limit secondary pollution, originating from the reagents applied for adsorbent surface modification, it is mandatory to apply environmentally-benign products (Gomez-Maldonado et al., 2019). In this context, phytic acid represents an interesting option to functionalize adsorbent surface, because of its eco-friendly nature and provides important active sites for heavy metals adsorption (You et al., 2016; Qin et al., 2017).

Carob (*Ceratonia Siliqua* L.) waste is an abundant material that has been studied for dye adsorption (Güzel et al., 2015; Reffas et al., 2016), but not yet examined for heavy metal removal. This study aimed at the valorization of carob waste for Cr(VI) elimination and assess the impact of its surface functionalization with phytic acid on the adsorption process. The modified material with an eco-friendly agent like phytic acid was used for the first time as an adsorbent for Cr(VI) removal. A systematic investigation of the effects of adsorbate concentration, contact time, adsorbent dose, pH and temperature on the adsorption process of Cr(VI) onto untreated and phytic acid-treated carob waste was undertaken.

2. Materials and methods

2.1. Materials

Carob (*Ceratonia Siliqua* L.) waste was obtained from carob factory in Bejaia, Algeria. Sodium hydroxide (NaOH), potassium dichromate ($K_2Cr_2O_7$), and phytic acid (PA) were procured from Sigma-Aldrich and used as-received. Hydrochloric acid (HCl) was obtained from Fisher scientific. Sodium chloride (NaCl), sodium nitrate ($NaNO_3$), sodium sulphate (Na_2SO_4), and trisodium orthophosphate dodecahydrate ($Na_3PO_4.12H_2O$) were purchased from Biochem.

2.2. Adsorbent preparation

The carob waste was already crushed into pieces of 2 cm in length and removed from its seeds by the factory. In the laboratory, the carob waste was dried at 80 °C overnight, and ground to fine particles using a disk mill. Then, part of the obtained powder was rinsed copiously with distilled water to eliminate the color and the soluble substances, dried for 24 h at 80 °C and stored for further use (named as CW).

2.3. Modification with phytic acid

Phytic acid-modified carob waste (PA-CW) was obtained by the same method used in (You et al., 2016; Qin et al., 2017). In short, 2 g of dry CW was placed in 30 mL of Milli-Q water and ultrasonicated for 30 min. Then, 1.2 g of urea and 2.1 mL of phytic acid were added and the resulting mixture was kept under magnetic stirring for 3 h at 60°C. After cooling to room temperature and centrifugation, the resulting powder was rinsed copiously with Milli-Q water to neutral pH and three times with ethanol. Finally, the material was dried for 24 h at 60°C and stored for further use.

2.4. Adsorption tests and regeneration

The adsorption experiments were conducted using the well-known and commonly used batch method, owing to its simple design. The tests were performed in conical flasks containing 50 mL of the Cr(VI) solution and varying the pH, adsorbent amount and the Cr(VI) concentration for an equilibrium time of 120 min at 25 °C. The mixture was shacked at 300 rpm. After each experiment, the sample was withdrawn, the adsorbent was isolated by centrifugation (13000 rpm) during 3 min and the supernatant was analyzed using UV-visible spectrophotometry at the λ_{max}=348 nm to assess the residual Cr(VI) concentration. The obtained data allowed to calculate the adsorption capacity (q_t, mg/g) and the amount of Cr(VI) removal (R) using the following equations:

$$q_t = \frac{(C_i - C_t)}{m} * V \qquad (1)$$

$$R(\%) = \frac{(C_i - C_t)}{C_i} * 100 \qquad (2)$$

where C_i and C_t are respectively the Cr(VI) initial and equilibrium concentration (mg/L), V denotes the volume (L) and m represents the mass of the adsorbent (g).

Adsorption kinetics and isotherms were studied in 200 mL beakers containing 100 mL of different Cr(VI) concentrations and 0.1 g of CW or 0.05 g of PA-CW at pH 2 and 25°C. Samples of 1.5 mL were taken out the solution at different time intervals to follow the remaining Cr(VI) by the same method mentioned above. All experiments were acquired in triplicate under the same experimental conditions to validate the empirical data.

The reusability of the adsorbents was assessed using the optimum parameters ([Cr(VI)]=100 mg/L, V=50 mL, [CW]=0.05 g or [PA-CW]=0.025 g, pH=2 and 25°C). After 120 min adsorption, Cr(VI) desorption was carried out using a solution of NaOH (0.1 M) under shaking for 4 h. These optimum parameters were maintained constant for each cycle.

2.5. Influence of co-existing anions

The effect of interfering anions like Cl^-, NO_3^-, SO_4^{2-} and PO_4^{3-} (100 mg/L) on Cr(VI) adsorption was studied using the optimum parameters ([Cr(VI)]=100 mg/L, V=50 mL, [CW]=0.05 g or [PA-CW]=0.025 g, pH=2, contact time=120 min, T=25°C).

3. Results and discussion

3.1. Characterization of CW and PA-CW

Fig. 1a and **S1** depict the crystal structure of raw CW, CW and PA-CW samples. The XRD pattern of raw CW reveals two main peaks at 14.73° and 21.86° attributed to the presence of cellulose (**Fig. S1**). In addition to cellulose peaks, the spectrum exhibits only a few sharp peaks, signifying that the pretreatment removed most of the impurities.

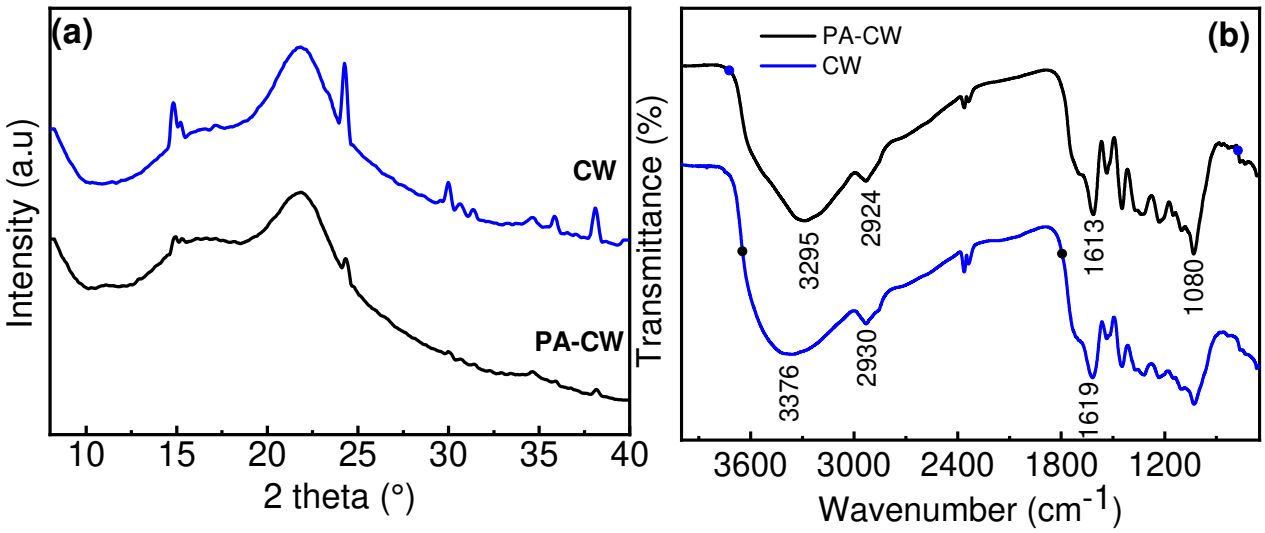

Figure 1. (**a**) XRD patterns of CW (blue) and PA-CW (black); (**b**) FTIR spectra of CW (blue) and PA-CW (black).

The diffractogram of PA-CW comprises the typical cellulose peaks at 14.73° and 21.86° quite similar to the CW precursor. From these results, it can be inferred that the pretreatment and phytic acid modification of the CW reduced its crystallinity, meaning that the obtained

adsorbents are of amorphous nature. This characteristic is suitable for an effective adsorption process (Güzel et al., 2015). Indeed, it has been observed that crystallinity affects the adsorption capacity, the pollutant tends to adsorb onto amorphous regions rather than onto crystalline ones (Gomez-Maldonado et al., 2019).

As seen in **Fig. 1b**, the FTIR plot of the CW displays many functional groups. It comprises bands between 3280 and 3380 cm^{-1} which refer to OH stretching, and bands at 2930 cm^{-1} attributed to C-H of aliphatic groups. The peak at 1619 cm^{-1} is due to stretching vibrations of C=O in the conjugated aldehyde and carboxylic acid groups, and the peak at 1447 cm^{-1} may be attributed to the C=O stretching in amide moiety. Besides, the bands at 1537 and 1231 cm^{-1} may be ascribed respectively to C=N and N-H stretching vibrations (Pradhan et al., 2019). The FTIR spectrum of PA-CW reveals roughly similar features with a slight shift of the characteristic wavenumbers due to phytic acid treatment. Furthermore, this treatment is approved in comparison to FTIR plot of phytic acid, which shows peaks at 1080 and 1120 cm^{-1} attributed respectively to the stretching of P=O and P-O (Jahan et al., 2018). Nevertheless, these peaks are also present in the CW spectrum at lower intensities, suggesting the presence of phosphate groups before the phytic acid treatment.

The results of thermal analysis of CW revealed three mass losses (**Fig. S2**). The first mass loss is related to the vaporization of free water at 100 °C, followed by two mass losses at 250 and 320 °C due respectively to cellulose and hemicellulose degradation. Furthermore, a slow decomposition of lignin occurred at above 400 °C. Similar thermal behavior was observed for PA-CW with a slight difference in the mass loss proportion related to the phytic acid (**Fig. S2**). Quite similar interpretations were described by many researchers on agricultural waste (Djilani et al., 2012; Sanchez-Silva et al., 2012).

The XPS survey spectra (**Fig. S3**) of CW and PA-CW samples confirmed the results of FTIR by the presence of peaks due to phosphorus, carbon, nitrogen and oxygen at 136, 285,

400 and 532 eV, respectively (Sherwood, 2002; Ali et al., 2020). The atomic concentrations of P_{2p}, C_{1s}, N_{1s} and O_{1s} in CW are 0.99, 79.10, 0.93 and 18.98 at%, respectively. For PA-CW, the atomic concentrations of P_{2p}, C_{1s}, N_{1s} and O_{1s} were respectively 1.81, 72.30, 1.85 and 24.03 at%. The increase in O, N and P proportions after treatment is related to phosphate and amine groups derived from phytic acid and urea.

The deconvolution of the core level of the C_{1s} of CW depicts four sets at 284.5 eV (63%), 286.0 eV (25%), 287.2 eV (9%) and 288.7 eV (3%), **Fig. 2**. Theses sets are attributed respectively to C-C, C-O, C=O and C-OOH (Tadjenant et al., 2020). The O_{1s} plot can be deconvoluted into three components at 530.8 eV (5%), 532.5 eV (90%) and 533.8 eV (5%) corresponding respectively to C-OH, -C=O and P-OH groups (Ali et al., 2020). The N_{1s} band of CW is curve-fitted with two components at 399.6 eV (79%) and 401.3 eV (21%) attributed respectively to free $-NH_2$ and protonated amine group $-NH_3^+$ (Kehrer et al., 2019).

Similarly, the C_{1s} of PA-CW could be deconvoluted into four features at 284.5 eV (56%), 286.0 eV (28%), 287.2 eV (10%) and 288.7 eV (6%) related respectively to C-C, C-O and C-OOH. The O_{1s} of PA-CW could be curve-fitted with two components at 530 eV (6%), 532.5 eV (89%) and 533.8 eV (5%) due respectively to C-H, C=O, and P-OH moieties. The deconvolution of the N_{1s} of PA-CW reveals two sets of peaks at 399.6 eV (87%) and 401.3 eV (13%) ascribed respectively to $-NH_2$ and protonated amine $–NH_3^+$.

The specific surface area and porosity are important characteristics for an effective adsorption, because they reflect the amount of active sites to retain the adsorbate (Almendros et al., 2015). These features are determined by the standard BET method, which is used for a wide range of fine powders and porous materials (Rouquerol et al., 2013). The N_2 adsorption-desorption isotherms revealed that the isotherm has a type IV shape, according to the IUPAC (International Union of Pure and Applied Chemistry) classification, characterized by an hysteresis loop of H_3-type related to non-rigid aggregates of plate-like particles (**Fig. S4**)

(Thommes et al., 2015). The surface area obtained for CW is 0.21 m^2/g; this value is enhanced

211 by the phytic acid treatment to reach 4.1 m²/g for PA-CW. Literature data reported surface

212 areas (0.5 < S_{BET} <

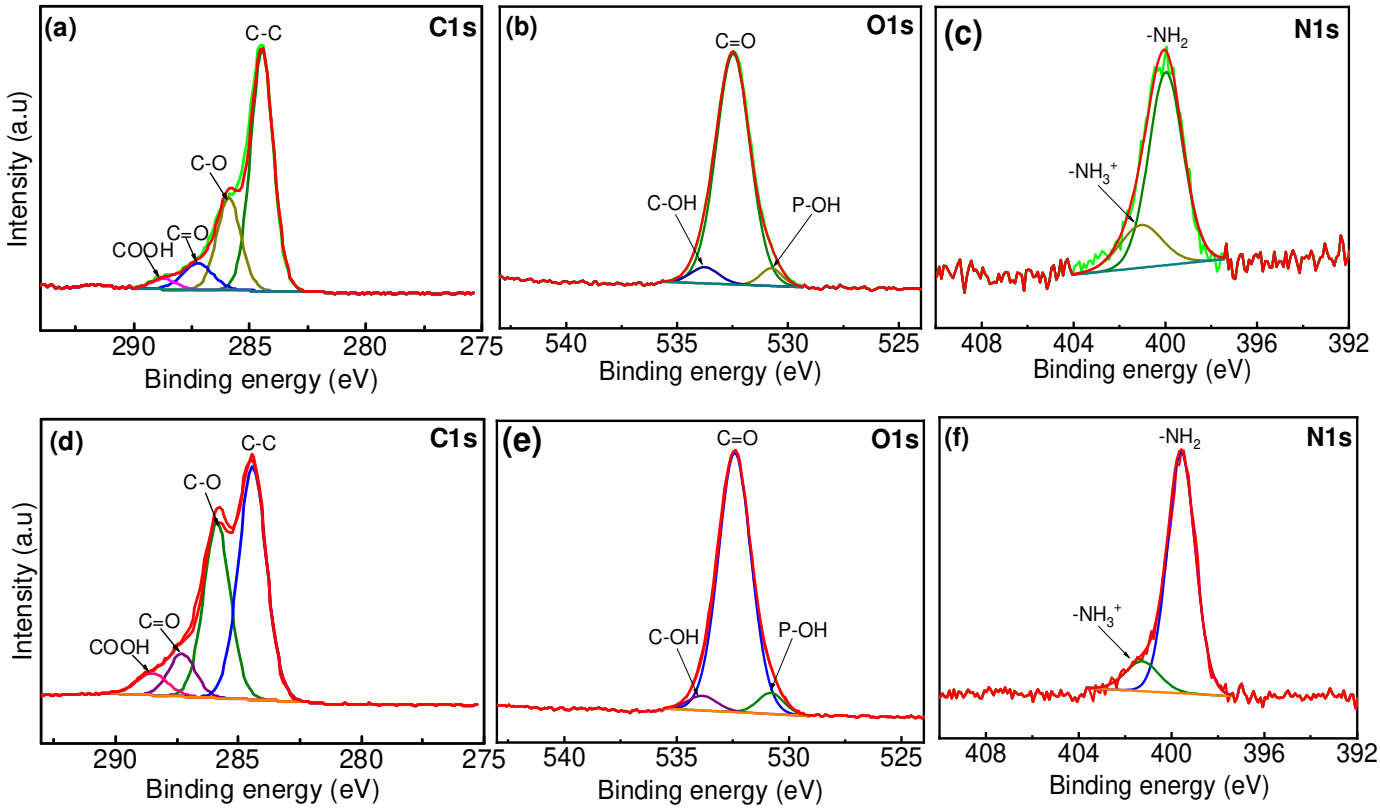

213 5 m^2/g) for agricultural waste used as adsorbents (Almendros et al., 2015).

214

215 **Figure 2.** Core level plots of (**a**) C_{1s}, (**b**) O_{1s}, (**c**) N_{1s} of CW; (**d**) C_{1s}, (**e**) O_{1s}, (**f**) N_{1s} of PA-
216 CW.

217 **3.2. Adsorption study**

218 **3.2.1. Influence of pH**

219 The pH of the solution and resulting surface charge of the adsorbent have an important
220 impact on the adsorption mechanism (Rouquerol et al., 2013). The effect of pH (**Fig. S5**) on
221 the adsorption process was investigated at constant Cr(VI) concentration (100 mg/L) and
222 adsorbent amount (0.05 g/CW and 0.025 g/PA-CW) at 25 °C in the range of pH 2 to 8. For
223 both CW and PA-CW, the optimum pH was found to be 2 with an adsorption capacity of 98.0
224 and 196.5 mg/g, respectively. Thereafter, a sharp decrease was evidenced for Cr(VI) removal
225 by CW, when the pH was increased. However, a clear reduction of the adsorption capacity to
226 78.8 mg/g was noticed at pH≈4. For instance, this contrasts with PA-CW which exhibited
227 only a slight decrease of the adsorption capacity (~6 mg/g) at pH≈4. The higher adsorption
228 capacity observed using PA-CW compared to CW could be explained by the presence of
229 more additional actives sites like –OH, P=O and $–NH_2$ after phytic acid treatment in presence
230 of urea. In other words, at low pH, the predominant species present in the solution are $HCrO_4^-$
231 (Zou et al., 2015), which are attracted to the positive sites formed by protonation of surface
232 moieties like amine, carboxyl and hydroxyl groups (Sathvika et al., 2019). Whereas at high
233 pH, repulsion forces occurred between the anionic molecules of the adsorbate and the
234 negatively charged surface, leading to adsorption capacity decrease (Kan et al., 2017).

235 The results were further validated by the determination of the point zero charge (PZC), as
236 shown in **Fig. S6**. The PZC values recorded for CW and PA-CW are respectively 5.4 and 4.4.
237 At $pH<pH_{PZC}$, the adsorbent surface is charged positively by the combination of excessive

protons (Dong et al., 2018), leading to enhanced adsorption capacity at low pH values of the dominant $HCrO_4^-$ species present in the solution phase. At $pH>pH_{PZC}$, the surface becomes negatively charged and a decline of adsorption capacity was obvious. These observations are in favor of Cr(VI) adsorption through electrostatic interactions between the negatively charged chromium species (Eqs. 3-6) and the positively charged adsorption sites, resulting from the protonation of the hydroxyl, phosphonate and amine groups on the adsorbent surface.

The equilibrium reactions of different Cr(VI) species in aqueous media are summarized below:

$$H_2CrO_4 \leftrightarrow HCrO_4^- + H^+ \quad (3)$$

$$Cr_2O_7^{2-} + H_2O \leftrightarrow 2HCrO_4^- \quad (4)$$

$$HCrO_4^- \leftrightarrow CrO_4^{2-} + H^+ \quad (5)$$

$$HCr_2O_7^- \leftrightarrow Cr_2O_7^{2-} + H^+ \quad (6)$$

3.2.2. Influence of initial concentration and contact time

Fig. S7 exhibits the study of contact time for different Cr(VI) concentrations (50-300 mg/L) at constant pH (2), and temperature (25±2°C). The adsorption capacity increases rapidly upon elevating the Cr(VI) concentration in the first 90 min, then slows down till it reaches equilibrium at 120-180 min. This could be ascribed to the presence of available sites on the adsorbent at the beginning (Khan et al., 2017). Thus, a contact time of 120 min was selected as an equilibrium contact time, since longer times were not effective in improving the adsorption capacity.

Furthermore, increasing the concentration of Cr(VI) from 50 to 300 mg/L causes an enhancement in the adsorption capacity from 47.0 to 247.0 mg/g for CW and from 95.3 to 411.1 mg/g for PA-CW. This significant increase might be due to the maximum driving force provided by the elevation of Cr(VI) concentration to face the mass transfer resistance of metal

263 ions due to collision with active sites during the adsorption process (Kuppusamy et al., 2016).

264 The same results were observed in previous studies (Saka et al., 2012; Yagub et al., 2014).

265 ### 3.2.3. Effect of adsorbent dose

The influence of adsorbent dose was studied in 100 mL conical flasks using 50 mL of fixed

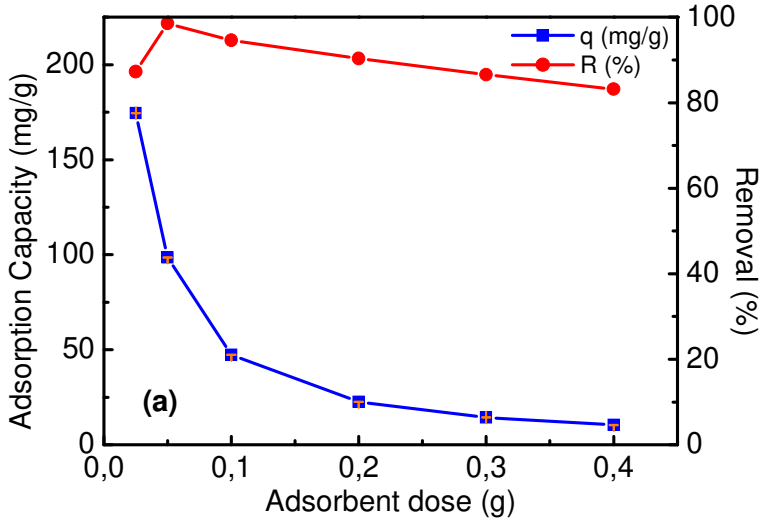

concentration (100 mg/L) of Cr(VI) at pH 2 and 25±2°C. The results in **Fig. 3** revealed that the highest percentage of Cr(VI) elimination was achieved using 0.05 and 0.025 g of CW and PA-CW with an adsorption capacity of 98.6 and 195.6 mg/g, respectively. Thereafter, increasing of the adsorbent amount from 0.025 to 0.4 g caused a decline of the adsorption capacity from 181.7 to 10.4 mg/g for CW and from 195.6 to 10.3 mg/L for PA-CW. This is most likely due to the agglomeration of the biomass particles, and also to the presence of more adsorbent than what it is necessary to remove the totality of the adsorbate (Ahmad et al., 2017; Pradhan et al., 2019). On the other hand, an increase of the efficiency was observed from 0.025 to 0.5 g in the case of CW, owing to the availability of exchangeable sites for ion metals. Then a weak decline was noticed for both adsorbents upon increasing the adsorbent dose due to the hidden sites, resulting from the reduction of the effective specific surface area (Tadjenant et al., 2020).

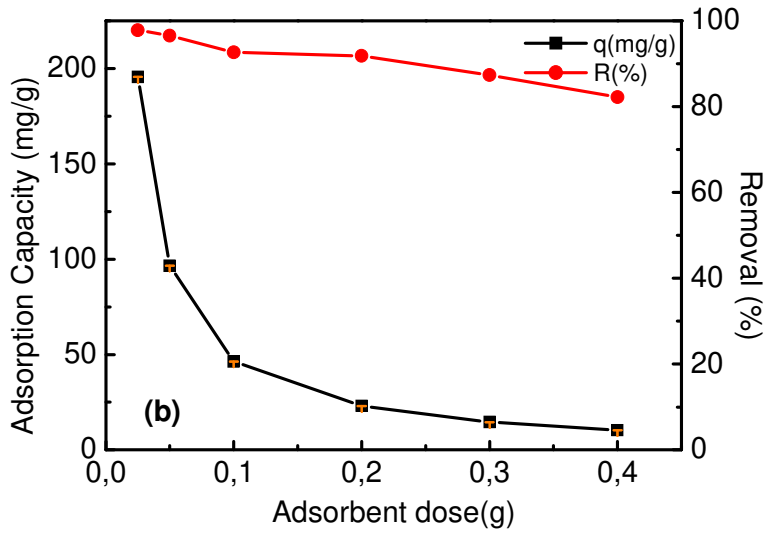

Figure 3. Influence of adsorbent dose on Cr(VI) removal by (**a**) CW and (**b**) PA-CW.

3.2.4. Effect of temperature

The influence of temperature on Cr(VI) removal was assessed using 100 mg/L of Cr(VI) solution, 0.1 g of CW or 0.05 g of PA-CW at pH 2 and various temperatures (25, 35 and 45°C) for a contact time of 180 min. As observed in **Fig. S8**, there is no difference in adsorption capacity equilibrium even at high temperature. Though the difference was observed on the equilibrium itself, it was achieved faster at 45°C (60 min) rather than at 35°C (90 min) and 25°C (120 min). This could be due to an increase of the adsorbent particles or the mobility of metal ions, resulting from the rise of temperature that provides a decrease of the viscosity of the solution (Güzel et al., 2015; Nasseh et al., 2017).

3.3. Data modeling

3.3.1. Kinetic modeling

Kinetic models are investigated to study the mechanism controlling the adsorption process, like mass transfer, residence time and sorption reactions (Ho and McKay, 1999)

using Laggragen (Ahmad et al., 2017), fist-order and second-order models expressed by the relationships (7, 8) :

$$\ln(q_t - q_e) = lnq_e - k_1 t \quad (7)$$

$$\frac{t}{q_t} = \frac{1}{k_1 q_e} + \frac{t}{q_e} \quad (8)$$

Where q and q_e represent the amounts (g) of solute sorbed per gram of adsorbent at any time and at equilibrium, respectively, and $k_1\ (min^{-1})$ and $k_2\ (g.mg^{-1}.min^{-1})$ denote respectively the rate constants of the first-order and second-order.

The results obtained from the kinetic modeling are summarized in **Fig. 4, Tables S1** and **S2**. The experimental values of adsorption capacity are closer to the ones found using the second order model and the plots were linear with good correlation coefficients. Therefore, it is considered that pseudo second order is an adequate model, which better fits the Cr(VI) adsorption process onto both CW and PA-CW, as initially described for low initial concentrations (Ho and McKay, 1999; Azizian, 2004a).

Intra-particle diffusion model

Intra-particle diffusion model expresses the relation between the adsorption capacity and the square of time given by Webber and Morris equation:

$$q_t = k_{id} t^{1/2} + C \quad (9)$$

Where $k_{id}(mg.g^{-1}\ min^{-1/2})$ denotes the intra-particle diffusion rate constant and $C\ (mg.g^{-1})$ represents a constant related to the thickness of the boundary layer. This model describes the mechanism of the particle diffusion through specific pores and the rate limiting step (Largitte and Pasquier, 2016). The intra-particle diffusion is the rate limiting sequence of the adsorption only if the plot of $q_t vs\ t^{1/2}$ is a straight line, which crosses the origin (Ofomaja, 2010).

Two straight portions are noticed (**Fig. S9**), suggesting that the intra-particle diffusion is not the only step controlling the adsorption process. The first segment refers to the external diffusion through macropores and the second segment corresponds to the internal diffusion through micropores (Güzel et al., 2015). The values of the constant k_{d1} are higher than those of k_{d2} (refer to **Table S3** and **S4**) due to the important diffusion from the solution to the intra-particle regions during the first stage, unlike to the second stage where the Cr(VI) concentration gradient dropped significantly (Tadjenant et al., 2020).

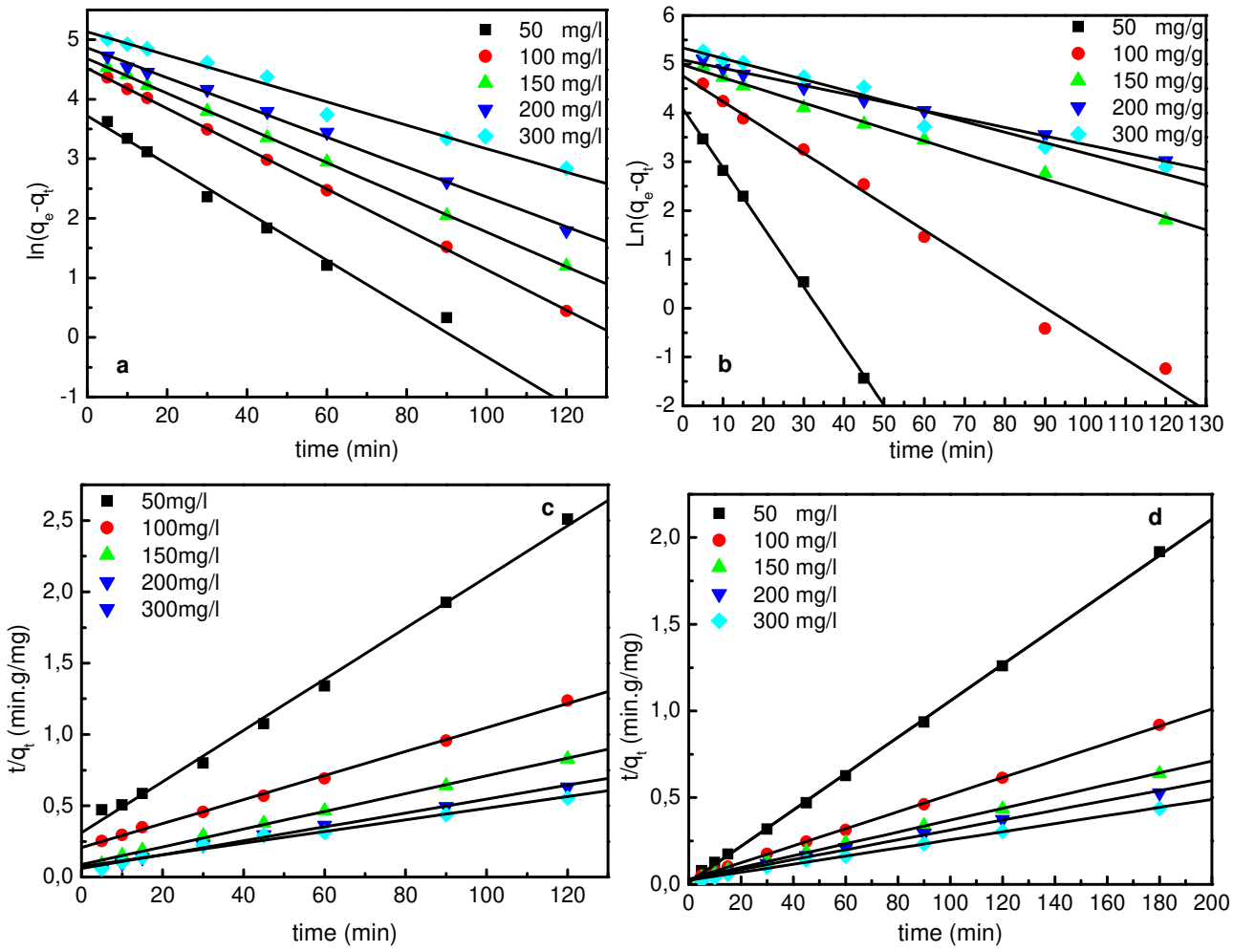
a
50 mg/l
100 mg/l
150 mg/l
200 mg/l
300 mg/l
ln(qe-qt)
time (min)
b
50 mg/g
100 mg/g
150 mg/g
200 mg/g
300 mg/g
Ln(qe-qt)
time (min)
c
50mg/l
100mg/l
150mg/l
200mg/l
300mg/l
t/qt (min.g/mg)
time (min)
d
50 mg/l
100 mg/l
150 mg/l
200 mg/l
300 mg/l
t/qt (min.g/mg)
time (min)

338

Figure 4. The plots of pseudo-first order models of (**a**) CW, (**b**) PA-CW and pseudo-second order models of (**c**) CW and (**d**) PA-CW for Cr(VI) removal.

3.3.2. Isotherm modeling

To gain more information on the adsorption process, it is necessary to view the link between the amount adsorbed per unit mass of adsorbent (q_e) and the remaining concentration of the adsorbate (C_e) at equilibrium. Many theoretical models are developed to describe the adsorption isotherms. The most known ones are Langmuir and Freundlich (Rangabhashiyam et al., 2014). For many years, the Langmuir model adapted is the classical one used to describe the adsorption from gas phase. It consists of monolayer adsorption with one kind of adsorbing sites, which can accommodate only one adsorbate molecule, and also assumes that there is no interaction between the adsorbed molecules, thus the adsorption energy is constant (Ruthven, 1984). A revised form of the Langmuir model was proposed in 2018. It provides an insight on the nature of adsorption and desorption processes in condensate phases (Azizian et al., 2018). This model is expressed as:

$$\frac{C_e}{q_e} = \frac{C_s}{K_{ML} q_m} + \frac{(k_{ML}-1)C_e}{K_{ML} q_m} \qquad (10)$$

Where C_s denotes the saturation concentration of Cr(VI) in liquid phase ($45\ mg.L^{-1}$), q_m the maximum adsorption capacity and K_{ML} is the constant of modified Langmuir.

Hence, the commonly multilayer model used is Freundlich model. It assumes heterogeneous surface and possible interactions between the adsorbed species (Rouquerol et al., 2013; Hussain and Kharisov, 2016). It is expressed as:

$$lnq_e = lnK_f + \frac{1}{n} lnC_e \qquad (11)$$

Where K_f and n correspond to the Freundlich constant related to the adsorption capacity and adsorption intensity, respectively.

From the results illustrated in the **Table S5** and **Fig. 5**, it could concluded that the Cr(VI) adsorption onto CW and PA-CW follows the modified Langmuir model with a maximum adsorption capacity of 212.4 and 387.9 mg/g, respectively.

A comparison of the adsorption capacities of Cr(VI) onto some natural adsorbents and the one obtained from this study is depicted in **Table 1**. It could be clearly seen that Cr(VI) adsorption onto CW and PA-CW are among the most effective processes realized in a short time.

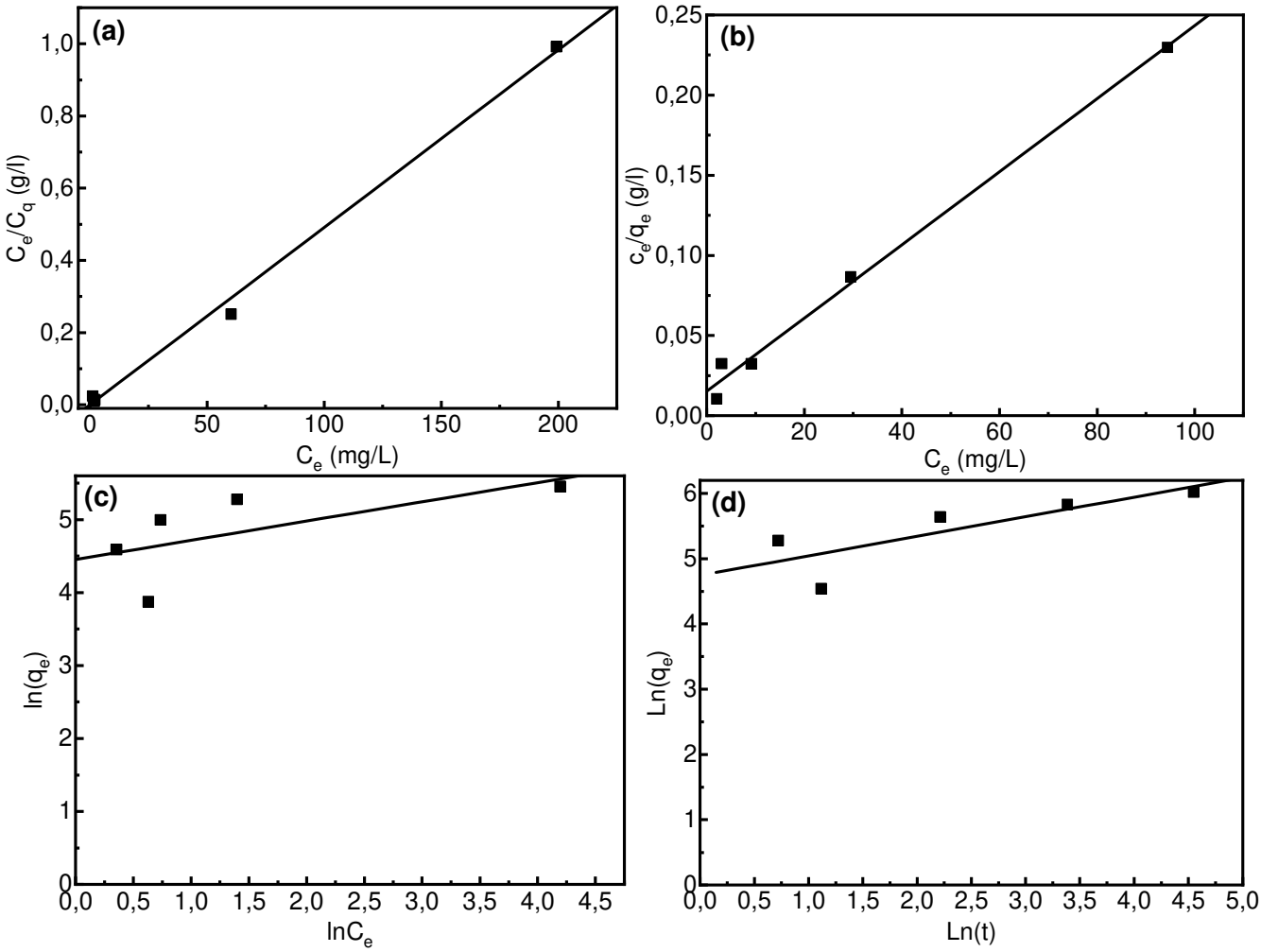

371

372 **Figure 5.** Langmuir model (**a**) CW, (**b**) PA-CW; Freundlich model (**c**) CW, (**d**) PA-CW for
373 Cr(VI) adsorption.

374

375 **Table 1.** Comparison between results recorded for Cr(VI) adsorption onto carob waste (CW)
376 and phytic acid-treated CW to the results of previous studies on natural adsorbents.

Adsorbent	**q_{max} (mg/g)**	**Kinetic model**	**Isotherm model**	**Contact time (min)**	**pH**	**Reference**
PA-CW	387.9	2^{nd} order	Langmuir	120	2	**This study**
CW	212.4	2^{nd} order	Langmuir	120	2	**This study**
Pistachiohull	116.6	2^{nd}order	Langmuir	70	2	(Moussavi and Barikbin, 2010)
Tea waste	90.9	2^{nd}oredr	Langmuir	240	3.9	(Nigam et al., 2019)
Melaleuca diosmifolia	62.5	2^{nd}order	Langmuir	420	2-3	(Kuppusamy et al., 2016)
Acidically prepared rice husk carbon	47.6	2^{nd} order	Langmuir-Freundlich	120	2	(Khan et al., 2016)
Activated carbon from fox nutshell	46.2	2^{nd} order	Langmuir	60	2	(Kumar and Jena, 2017)
Gliricidiasepium leaf powder	35.7	2^{nd} order	Freundlich	160	2	(Suganya et al., 2019)
Banana Peel Crambery Rosehup seed shell	10.4 15.2 6.8	2^{nd} order	Langmuir and Dubivin-Radeskevich	60	2	(Parlayici and Pehlivan, 2019)
Sunflowers	7.9	2^{nd} order	Langmuir	120	2	(Jain et al., 2013)
Amalta leaves Peanut shell	4.5 4.3	2^{nd} order	Langmuir	360	4	(Ahmad et al., 2017)

377

378 **3.3.3. Thermodynamic study**

The determination of thermodynamic factors such as free energy $\Delta G°$, enthalpy $\Delta H°$ and entropy $\Delta S°$ allows to qualify the spontaneity of the adsorption process and the nature of energy (exothermic or endothermic) (Pradhan et al., 2019). These parameters are given by the following equations:

$$K_d = \frac{q_e}{C_e} \quad (12)$$

$$\Delta G° = -RTlnK_d \quad (13)$$

$$\Delta G° = \Delta H° - T.\Delta S° \quad (14)$$

$$lnK_d = \frac{\Delta S°}{R} - \frac{\Delta H°}{R}.\frac{1}{T} \quad (15)$$

Where T corresponds to the adsorption temperature (K) and R denotes the universal gas constant $(J.mol^{-1}K^{-1})$. From the data in **Figure S10** and **Table S6**, it could be deduced that the process of Cr(VI) uptake is spontaneous and physical, owing to the negative charge preceding the value of $\Delta G°$ which is less than 20 KJ/mol (Güzel et al., 2015).

Moreover, the negative value of $\Delta H°$ reveals that the nature of the adsorption is exothermic. Whereas, the entropy $\Delta S°$ infers the randomness of the adsorbate molecules on the surface of the adsorbent.

3.3.4. Cr(VI) removal mechanism

XPS analysis (**Fig. 6**) gives valuable information on the valence state of species on the adsorbent surface before and after adsorption. The Cr_{2p} high-resolution XPS plots of the CW **(Fig. 6a)** and PA-CW **(Fig. 6b)** after adsorption process revealed peaks ascribed to $Cr_{2p1/2}$ and $Cr_{2p3/2}$ respectively at 588 and 579 eV associated with Cr(VI). Furthermore, the optimum fitting after deconvolution of Cr_{2p} spectrum revealed two additional components at 575 and 585 eV ascribed to Cr(III) (Tadjenant et al., 2020). The results clearly suggest that Cr(VI) adsorption is accompanied by its reduction to Cr(III). It is important to notice that Cr(III) represents the highest portion on both adsorbents' surface (PA-CW: 88% and CW: 66%).

Therefore, Cr(VI) reduction to Cr(III) was higher using PA-CW than CW although both of them are good adsorbents for Cr(VI) elimination.

In addition, deconvolution of the C_{1s} of CW and PA-CW, after Cr adsorption (**Fig. S11**), revealed the presence of a peak at 282.9 eV ascribed to C-Cr bond (Folkenant et al., 2015). This peak, absent in the C_{1s} of the initial adsorbent materials, accounts for 13% and 19% after Cr(VI) adsorption on respectively CW and PA-CW. In addition, the overall contributions of different carbon moieties (C-OH, C=O and COOH) before and after Cr(VI) adsorption did not vary significantly, while the C-H/C-C contribution decreased by about 18% and 11% for CW and PA-CW, respectively (**Table S7**). Taken together, these results suggest that Cr(VI) reduction took place through C-H sequential oxidation, as previously suggested by Zhuang et al. (Zhuang et al., 2014) even though their XPS results did not provide any evidence for the presence of C-Cr bonds.

Cr(VI) removal occurred by adsorption, reduction and/or adsorption-reduction, owing to the different functional groups present on the adsorbent surface, as illustrated by XPS analysis in **Fig. 2**. Cr(VI) reduction requires $3e^-/7H^+$ (Eq. 16), signifying that this process is favorable in acidic media.

$$HCrO_4^- + 7H^+ + 3e^- \longrightarrow Cr^{3+} + 4\ H_2O \qquad E^0 = +1.35\ V \qquad (16)$$

XPS analysis provided a convincing evidence on Cr(VI) reduction to Cr(III) ions and their adsorption of the adsorbents' surface. The appearance of C-Cr species in the C_{1s} XPS plot indicates the involvement of C-H bond oxidation during Cr(VI reduction to Cr(III).

Cr(VI) elimination occurred directly through Cr(VI) anions binding onto the positively charged surface moieties of the adsorbents (Ads) involving electrostatic interactions (Eqs. 17-19) (Park et al., 2008).

$$Ads\text{-}NH_2(s) + HCrO_4^-\ (aq) + H^+\ (aq) \leftrightarrow Ads\text{-}NH_3^+ \ldots HCrO_4^-(s) \qquad (17)$$

$$\text{Ads-COOH(s)} + HCrO_4^- \text{ (aq)} + H^+ \text{ (aq)} \leftrightarrow \text{Ads-COOH}_2^+ \ldots HCrO_4^- \text{(s)} \quad (18)$$

$$\text{Ads-H}_2PO_4\text{(s)} + HCrO_4^- \text{ (aq)} + H^+ \text{ (aq)} \leftrightarrow \text{Ads-H}_3PO_4 \ldots HCrO_4^- \text{(s)} \quad (19)$$

Whereas Cr(VI) reduction to Cr(III) took place through electron donor groups provided on the surface; it is not excluded that a fraction of the reduced Cr(III) species may be released to the aqueous phase due to electronic repulsion between the positively charged groups and Cr(III), or complexed with adjacent groups (Eqs. 20-24) (Park et al., 2008; Jahan et al., 2018).

$$\text{-C-H} + \text{Cr(VI)} + H_2O \rightarrow \text{-C-OH} + \text{Cr(III)} + H^+ \quad (20)$$

$$\text{-C-OH} + \text{Cr(VI)} \rightarrow \text{-C=O} + \text{Cr(III)} + H^+ \quad (21)$$

$$\text{-C=O} + \text{Cr(VI)} + H_2O \rightarrow \text{-COOH} + \text{Cr(III)} + H^+ \quad (22)$$

$$\text{C-COOH} + \text{Cr(VI)} \rightarrow \text{-C-Cr(III)} + CO_2 + H^+ \quad (23)$$

The released Cr(III) in solution may be linked to the deprotonated functional groups at higher pH (Jahan et al., 2018).

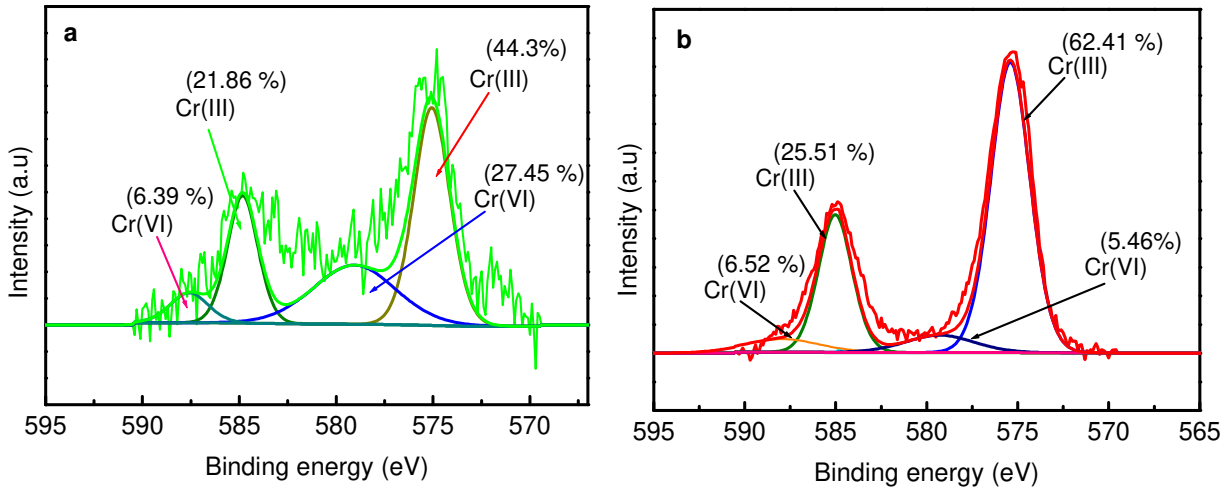

$$\text{Ads-COOH(s)} + Cr^{3+}\text{(aq)} \leftrightarrow \text{B-3(COO}^- \text{)} \ldots Cr^{3+} + 3H^+ \quad (24)$$

Figure 6. High resolution XPS plots of the Cr_{2p} of CW (**a**) and PA-CW (**b**) after Cr(VI) adsorption.

3.3.5. Desorption study and interfering anion effect

In order to assess the practical utility of CW and PA-CW, desorption tests were conducted. The regeneration of the adsorbents was performed up to 4 cycles using 0.1 M NaOH as the eluent agent (Hsini et al., 2021). The results in **Fig. 7a** indicate that the removal of Cr(VI) decreased upon increasing the number of cycles. The adsorption capacities of CW were found to be 55.1, 33.6, 28.7 and 25.1 mg/g, while those of PA-CW were determined to be 109.0, 70.7, 54.2 and 49.3 mg/g, respectively for the first, second, third and fourth cycles of Cr(VI) adsorption. The obtained data infer that, under our experimental conditions, the electrostatic interactions of Cr species with the adsorbents' surface are sufficiently strong to be displaced by 0.1 M NaOH, thus leading to only partial removal of the adsorbed chromium. Additional experiments are required to optimize the desorption conditions to achieve full regeneration of the surface i.e. total desorption of chromium species from the adsorbent surface.

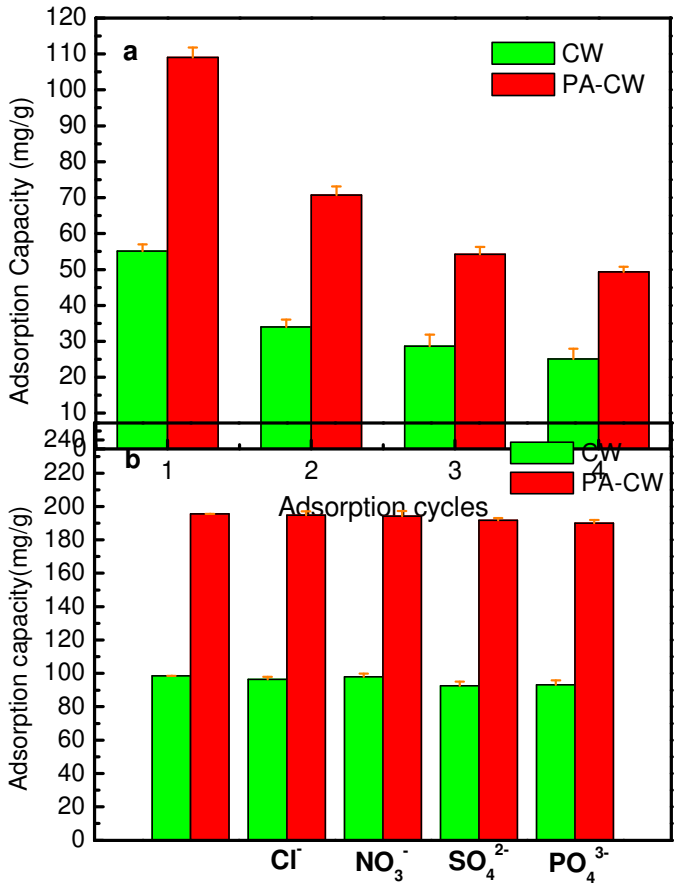

Figure 7. (**a**) Effect of regeneration cycles and (**b**) effect of interfering anions on the adsorption of Cr(VI) onto CW and PA-CW.

Furthermore, the influence of co-existing anions like Cl^-, NO_3^-, SO_4^{2-} and PO_4^{3-} on the Cr(VI) removal on both CW and PA-CW was investigated (**Fig. 7b**). The results revealed that these anions, when investigated at the same concentration as that of Cr(VI), did not have a significant impact on the adsorption capacity. Indeed, only a slight decrease (2 – 6 mg/g) of the adsorption capacity was recorded under our experimental conditions, suggesting the lack of competition of theses anions for binding the positively charged surface in presence of chromium anions or the electrostatic interactions of Cr(VI) with the positively charged binding sites on the adsorbents' surface are much stronger (Dong et al., 2018). The results corroborate the data of the regeneration study.

4. Conclusion

The adsorption of Cr(VI) onto carob waste (CW) is a low cost technique to reduce and remove this toxic contaminant. Our study demonstrated that agricultural CW can substitute the classical adsorbents, owing to its important adsorption capacity of 212.4 mg/g. Furthermore, the activation of the CW with phytic acid (PA) as an eco-friendly molecule improved the specific surface area from 0.21 m^2/g to 4.1 m^2/g and enhanced the adsorption capacity to 387.9 mg/g. The data gathered from different characterizations of CW and PA-CW like FTIR, XRD, TGA and BET showed that both adsorbents have the required

properties like amorphous structure, favorable porosity and specific surface area for a satisfying adsorption. The adsorption tests revealed that the optimum pH was 2 for both raw CW and PA-CW at 25°C for 2h as equilibrium contact time. The data of kinetic study fitted well the pseudo second order, whereas the isotherm modeling inferred that the modified Langmuir model is the adequate model describing the adsorption process. Besides, the thermodynamic results reflected that Cr(VI) adsorption onto CW and PA-CW is a spontaneous and a physical adsorption process. XPS analysis of CW and PA-CW after Cr(VI) adsorption evidenced that Cr(VI) was reduced to Cr(III), suggesting a reduction-adsorption mechanism. To sum up, carob and phytic acid-treated carob wastes are effective for Cr(VI) ions effective removal.

Acknowledgement

The authors gratefully acknowledge financial support of the Algerian ministry of high education scientific research for 7 months PROFAS B+ scholarship, the Centre National de la Recherche Scientifique (CNRS), the University of Lille and the Hauts-de-France region. The authors also thank the Taif University Researchers Supporting Project number (TURSP-2020/03), Taif University, Taif, Saudi Arabia.

References

Ahmad, A., Ghazi, Z.A., Saeed, M., Ilyas, M., Ahmad, R., Khattak, A.M., Iqbal, A., 2017. A comparative study of the removal of Cr(VI) from synthetic solution using natural biosorbents. New J. Chem. 41, 10799-10807.

Akpor, O.B., Ohiobor, G.O., Olaolu, T.D., 2014. Heavy metal pollutants in wastewater effluents: sources, effects and remediation. Adv. Biosci. Bioeng. 2, 37-43.

Ali, M.B., Wang, F., Boukherroub, R., Xia, M., 2020. High performance of phytic acid-functionalized spherical poly-phenylglycine particles for removal of heavy metal ions. Appl. Surf. Sci. 518, 146206.

513 Almendros, A., Martín-Lara, M., Ronda, A., Pérez, A., Blázquez, G., Calero, M., 2015.
514 Physico-chemical characterization of pine cone shell and its use as biosorbent and fuel.
515 Bioresource Technol. 196, 406-412.
516 Azizian, S., 2004. Kinetic models of sorption: a theoretical analysis. J. Colloid Interface Sci.
517 276, 47-52.
518 Azizian, S., Eris, S., Wilson, L.D., 2018. Re-evaluation of the century-old Langmuir isotherm
519 for modeling adsorption phenomena in solution. Chem. Phys. 513, 99-104.
520 Babarinde, A., Onyiaocha, G.O., 2016. Equilibrium sorption of divalent metal ions onto
521 groundnut (Arachis hypogaea) shell: kinetics, isotherm and thermodynamics. Chem. Int. 2.
522 Chao, H.-P., Chang, C.-C., Nieva, A., 2014. Biosorption of heavy metals on Citrus maxima
523 peel, passion fruit shell, and sugarcane bagasse in a fixed-bed column. J. Ind. Eng. Chem. 20,
524 3408-3414.
525 Dehghani, M., Heibati, B., Asadi, A., Tyagi, I., Agarwal, S., Gupta, V., 2016. Reduction of
526 noxious Cr (VI) ion to Cr (III) ion in aqueous solutions using H_2O_2 and UV/H_2O_2 systems. J.
527 Ind. Eng. Chem. 33, 197-200.
528 Djilani, C., Zaghdoudi, R., Modarressi, A., Rogalski, M., Djazi, F., Lallam, A., 2012.
529 Elimination of organic micropollutants by adsorption on activated carbon prepared from
530 agricultural waste. Chem. Eng. J. 189, 203-212.
531 Dong, L., Liang, J., Li, Y., Hunang, S., Wei, Y., Bai, X., Jin, Z., Zhang, M., Qu, J., 2018.
532 Effect of coexisting ions on Cr (VI) adsorption onto surfactant modified Auricularia auricula
533 spent substrate in aqueous solution. Ecotoxicology and environmental safety 166, 390-400.
534 Folkenant, M., Nygren, K., Malinovskis, P., Palisaitis, J., Persson, P.O.Å., Lewin, E., Jansson,
535 U., 2015. Structure and properties of Cr–C/Ag films deposited by magnetron sputtering. Surf.
536 Coat. Technol. 281, 184-192.

Gomez-Maldonado, D., Erramuspe, I.B.V., Peresin, M.S., 2019. Natural polymers as alternative adsorbents and treatment agents for water remediation. BioResources 14, 10093-10160.

GracePavithra, K., Jaikumar, V., Senthil Kumar, P., SundarRajan, P.S., 2019. A review on cleaner strategies for chromium industrial wastewater: Present research and future perspective. J. Clean. Prod. 228, 580-593.

Güzel, F., Sayğılı, H., Sayğılı, G.A., Koyuncu, F., 2015. New low-cost nanoporous carbonaceous adsorbent developed from carob (Ceratonia siliqua) processing industry waste for the adsorption of anionic textile dye: characterization, equilibrium and kinetic modeling. J. Mol. Liq. 206, 244-255.

Halouane, F., Oz, Y., Meziane, D., Barras, A., Juraszek, J., Singh, S.K., Kurungot, S., Shaw, P.K., Sanyal, R., Boukherroub, R., 2017. Magnetic reduced graphene oxide loaded hydrogels: highly versatile and efficient adsorbents for dyes and selective Cr (VI) ions removal. J. Colloid Interface Sci. 507, 360-369.

Heidarinejad, Z., Dehghani, M.H., Heidari, M., Javedan, G., Ali, I., Sillanpää, M., 2020. Methods for preparation and activation of activated carbon: a review. Environ. Chem. Lett. 18, 393-415.

Ho, Y.-S., McKay, G., 1999. Pseudo-second order model for sorption processes. Process Biochem. 34, 451-465.

Hsini, A., Naciri, Y., Laabd, M., Bouziani, A., Navío, J., Puga, F., Boukherroub, R., Lakhmiri, R., Albourine, A., 2021. Development of a novel PANI@WO_3 hybrid composite and its application as a promising adsorbent for Cr (VI) ions removal. J. Environ.l Chem. Eng., 105885.

Hussain, C.M., Kharisov, B., 2016. Advanced environmental analysis: applications of nanomaterials. Royal Society of Chemistry.

562 Jahan, K., Kumar, N., Verma, V., 2018. Removal of hexavalent chromium from potable
563 drinking using a polyaniline-coated bacterial cellulose mat. Environ. Sci.: Water Res.
564 Technol. 4, 1589-1603.
565 Jain, M., Garg, V., Kadirvelu, K., 2013. Chromium removal from aqueous system and
566 industrial wastewater by agricultural wastes. Bioremediation J. 17, 30-39.
567 Jaishankar, M., Tseten, T., Anbalagan, N., Mathew, B.B., Beeregowda, K.N., 2014. Toxicity,
568 mechanism and health effects of some heavy metals. Interdisciplinary Toxicol. 7, 60-72.
569 Kan, C.-C., Ibe, A.H., Rivera, K.K.P., Arazo, R.O., de Luna, M.D.G., 2017. Hexavalent
570 chromium removal from aqueous solution by adsorbents synthesized from groundwater
571 treatment residuals. Sustain. Environ. Res. 27, 163-171.
572 Kehrer, M., Duchoslav, J., Hinterreiter, A., Cobet, M., Mehic, A., Stehrer, T., Stifter, D.,
573 2019. XPS investigation on the reactivity of surface imine groups with TFAA. Plasma
574 Processes Polym. 16, 1800160.
575 Khan, T., Isa, M.H., Mustafa, M.R.U., Yeek-Chia, H., Baloo, L., Manan, T.S.B.A., Saeed,
576 M.O., 2016. Cr (VI) adsorption from aqueous solution by an agricultural waste based carbon.
577 RSC Adv. 6, 56365-56374.
578 Khan, T.A., Nazir, M., Ali, I., Kumar, A., 2017. Removal of chromium (VI) from aqueous
579 solution using guar gum–nano zinc oxide biocomposite adsorbent. Arab. J. Chem. 10, S2388-
580 S2398.
581 Kumar, A., Jena, H.M., 2017. Adsorption of Cr (VI) from aqueous solution by prepared high
582 surface area activated carbon from Fox nutshell by chemical activation with H_3PO_4. J.
583 Environ. Chem. Eng. 5, 2032-2041.
584 Kuppusamy, S., Thavamani, P., Megharaj, M., Venkateswarlu, K., Lee, Y.B., Naidu, R.,
585 2016. Oak (Quercus robur) acorn peel as a low-cost adsorbent for hexavalent chromium
586 removal from aquatic ecosystems and industrial effluents. Water, Air, Soil Pollution 227, 62.

587 Kuppusamy, S., Venkateswarlu, K., Thavamani, P., Lee, Y.B., Naidu, R., Megharaj, M.,
588 2017. Quercus robur acorn peel as a novel coagulating adsorbent for cationic dye removal
589 from aquatic ecosystems. Ecological Eng. 101, 3-8.
590 Largitte, L., Pasquier, R., 2016. A review of the kinetics adsorption models and their
591 application to the adsorption of lead by an activated carbon. Chem. Eng. Res. Design 109,
592 495-504.
593 Li, F., Huang, J., Xia, Q., Lou, M., Yang, B., Tian, Q., Liu, Y., 2018. Direct contact
594 membrane distillation for the treatment of industrial dyeing wastewater and characteristic
595 pollutants. Sep. Purif. Technol. 195, 83-91.
596 Mishra, S., Bharagava, R.N., 2016. Toxic and genotoxic effects of hexavalent chromium in
597 environment and its bioremediation strategies. J. Environ. Sci. Health C 34, 1-32.
598 Moussavi, G., Barikbin, B., 2010. Biosorption of chromium (VI) from industrial wastewater
599 onto pistachio hull waste biomass. Chem. Eng. J. 162, 893-900.
600 Nasseh, N., Taghavi, L., Barikbin, B., Harifi-Mood, A.R., 2017. The removal of Cr (VI) from
601 aqueous solution by almond green hull waste material: kinetic and equilibrium studies. J.
602 Water Reuse Desalination 7, 449-460.
603 Nigam, M., Rajoriya, S., Singh, S.R., Kumar, P., 2019. Adsorption of Cr (VI) Ion from
604 Tannery Wastewater on Tea Waste: Kinetics, Equilibrium and Thermodynamics Studies. J.
605 Environ. Chem. Eng., 103188.
606 Ning, P., Lin, X., Cao, H., Zhang, Y., 2014. Selective extraction and deep separation of V (V)
607 and Cr (VI) in the leaching solution of chromium-bearing vanadium slag with primary amine
608 LK-N21. Sep. Purif. Technol. 137, 109-115.
609 Ofomaja, A.E., 2010. Intraparticle diffusion process for lead (II) biosorption onto mansonia
610 wood sawdust. Bioresource Technol. 101, 5868-5876.

611 Ouafi, R., Rais, Z., Taleb, M., Benabbou, M., Asri, M., 2017. Sawdust in the treatment of
612 heavy metals-contaminated wastewater. Environ. Res. J. 11.
613 Park, D., Lim, S.-R., Yun, Y.-S., Park, J.M., 2008. Development of a new Cr (VI)-biosorbent
614 from agricultural biowaste. Bioresource Technol. 99, 8810-8818.
615 Parlayici, Ş., Pehlivan, E., 2019. Comparative study of Cr (VI) removal by bio-waste
616 adsorbents: equilibrium, kinetics, and thermodynamic. J. Anal. Sci. Technol. 10, 15.
617 Pradhan, D., Sukla, L.B., Mishra, B.B., Devi, N., 2019. Biosorption for removal of hexavalent
618 chromium using microalgae *Scenedesmus sp*. J. Clean. Prod. 209, 617-629.
619 Qin, P., Xu, X., Cai, Y., Bai, B., Wang, H., Suo, Y., 2017. Fabrication of phytic acid-
620 modified wheat straw platform and its pH-responsive release performance for the pesticide
621 imidacloprid. RSC Adv. 7, 32777-32785.
622 Rangabhashiyam, S., Anu, N., Giri Nandagopal, M.S., Selvaraju, N., 2014. Relevance of
623 isotherm models in biosorption of pollutants by agricultural byproducts. J. Environ. Chem.
624 Eng. 2, 398-414.
625 Reffas, A., Bouguettoucha, A., Chebli, D., Amrane, A., 2016. Adsorption of ethyl violet dye
626 in aqueous solution by forest wastes, wild carob. Desalination Water Treat. 57, 9859-9870.
627 Rouquerol, J., Rouquerol, F., Llewellyn, P., Maurin, G., Sing, K.S., 2013. Adsorption by
628 powders and porous solids: principles, methodology and applications. Academic press.
629 Ruthven, D.M., 1984. Principles of adsorption and adsorption processes. John Wiley & Sons.
630 Saka, C., Şahin, Ö., Adsoy, H., Akyel, Ş.M., 2012. Removal of methylene blue from aqueous
631 solutions by using cold plasma, microwave radiation and formaldehyde treated acorn shell.
632 Sep. Sci. Technol. 47, 1542-1551.
633 Sanchez-Silva, L., López-González, D., Villaseñor, J., Sánchez, P., Valverde, J., 2012.
634 Thermogravimetric–mass spectrometric analysis of lignocellulosic and marine biomass
635 pyrolysis. Bioresource Technol. 109, 163-172.

636 Sathvika, T., Balaji, S., Chandra, M., Soni, A., Rajesh, V., Rajesh, N., 2019. A co-operative
637 endeavor by nitrifying bacteria Nitrosomonas and Zirconium based metal organic framework
638 to remove hexavalent chromium. Chem. Eng. J. 360, 879-889.
639 Schwantes, D., Gonçalves, A.C., Coelho, G.F., Campagnolo, M.A., Dragunski, D.C., Tarley,
640 C.R.T., Miola, A.J., Leismann, E.A.V., 2016. Chemical modifications of cassava peel as
641 adsorbent material for metals ions from wastewater. J. Chem. 2016, 3694174.
642 Sherwood, P.M.A., 2002. Introduction to studies of phosphorus-oxygen compounds by XPS.
643 Surf. Sci. Spectra 9, 62-66.
644 Suganya, E., Saranya, N., Patra, C., Varghese, L.A., Selvaraju, N., 2019. Biosorption potential
645 of Gliricidia sepium leaf powder to sequester hexavalent Chromium from synthetic aqueous
646 solution. J. Environ.Chem. Eng., 103112.
647 Tadjenant, Y., Dokhan, N., Barras, A., Addad, A., Jijie, R., Szunerits, S., Boukherroub, R.,
648 2020. Graphene oxide chemically reduced and functionalized with KOH-PEI for efficient Cr
649 (VI) adsorption and reduction in acidic medium. Chemosphere 258, 127316.
650 Thommes, M., Kaneko, K., Neimark, A.V., Olivier, J.P., Rodriguez-Reinoso, F., Rouquerol,
651 J., Sing, K.S., 2015. Physisorption of gases, with special reference to the evaluation of surface
652 area and pore size distribution (IUPAC Technical Report). Pure Appl. Chem. 87, 1051-1069.
653 Vasudevan, S., Lakshmi, J., 2011. Studies relating to an electrochemically assisted
654 coagulation for the removal of chromium from water using zinc anode. Water Science and
655 Technology: Water supply 11, 142-150.
656 Yagub, M.T., Sen, T.K., Ang, M., 2014. Removal of cationic dye methylene blue (MB) from
657 aqueous solution by ground raw and base modified pine cone powder. Environ. Earth Sci. 71,
658 1507-1519.

659 Ye, Y., Ren, Y., Zhu, J., Wang, J., Li, B., 2016. Removal of nitrate and Cr (VI) from drinking
660 water by a macroporous anion exchange resin. Desalination Water Treatment 57, 26427-
661 26439.
662 You, H., Chen, J., Yang, C., Xu, L., 2016. Selective removal of cationic dye from aqueous
663 solution by low-cost adsorbent using phytic acid modified wheat straw. Colloids Surf. A:
664 Physicochem. Eng. Aspects 509, 91-98.
665 Zhuang, L., Li, Q., Chen, J., Ma, B., Chen, S., 2014. Carbothermal preparation of porous
666 carbon-encapsulated iron composite for the removal of trace hexavalent chromium. Chem.
667 Eng. J. 253, 24-33.
668 Zou, Z., Tang, Y., Jiang, C., Zhang, J., 2015. Efficient adsorption of Cr (VI) on sunflower
669 seed hull derived porous carbon. J. Environ. Chem. Eng. 3, 898-905.

670

Graphical Abstract